CHAPTER 30

A Spectral Multi-Domain Technique Applied to High-Speed Chemically Reacting Flows

*Michele G. Macaraeg**
Craig L. Streett†
M. Yousuff Hussaini††

Abstract. The first applications of a spectral multi-domain method for viscous compressible flow are presented. The method imposes a global flux balance condition at the interface so that high-order continuity of the solution is preserved. The global flux balance is imposed in terms of a spectral integral of the discrete equations across adjoining domains. Since the discretized equations interior to each domain are solved uncoupled from each other and since the interface relation has a block structure, the solution scheme can be adapted to the particular requirement in each sub-domain. The multiple scales associated with chemically reacting flows and transition important areas for hypersonic research, are motivating applications well-suited for the present spectral multi-domain technique. The following work will focus on both of these topics which are rapidly gaining widespread attention in computational fluid dynamics. The discretization techniques implemented for solution of these two problems are distinctly different: a nonstaggered multi-domain

*Computational Methods Branch, High-Speed Aerodynamics Division, NASA Langley Research Center, Hampton, Virginia.
†Theoretical Aerodynamics Branch, Transonic Aerodynamics Division, NASA Langley Research Center, Hampton, Virginia.
‡Institute for Computer Applications and Scientific Engineering, Hampton, Virginia.

discretization is utilized for the calculation of the chemically reacting flow, and the first implementation of a staggered multi-domain mesh is presented to accurately solve the stability equations for a viscous compressible fluid. The successful implementation of the latter discretization is strongly dependent on the interface condition of a multi-domain technique. The global-flux balance condition of the present method poses no problem for staggered mesh calculations.

1. Introduction. A number of spectral domain decomposition techniques have appeared in the literature and are becoming accepted tools for fluid dynamical calculations. For example, the spectral element method which applies finite element methodology using Galerkin spectral discretization in the variational formulation within elements is a popular technique [1,2]. This technique utilizes a split Galerkin-collocation discretization which restricts its application to convection-diffusion problems for incompressible flows. The spectral element method in practice is used in a manner similar to classical finite element techniques: Low-order internal discretization using many elements with no internal stretchings to improve resolution. The technique is most easily implemented if each element utilizes the same number of collocation points. Other domain decomposition techniques involve explicit enforcement of C^1 continuity across the interface [3,4]. It is not clear how well these techniques perform for strongly convection-dominated problems; the second author's experience with such techniques [5] has shown them to be not entirely satisfactory.

The spectral multi-domain technique of the present paper was developed with compressible flow applications in mind. The multiple scales associated with chemically reacting flows and transition, both features of hypersonic aerodynamics, was a further consideration in developing the multi-domain technique. The former issue will be addressed by incorporating a nonequilibrium chemistry model for air into the spectral multi-domain Navier-Stokes solution method. The application will focus on the chemical kinetics initiated as air passes through a fully resolved shock wave.

2. Spectral Multi-Domain Technique. Spectral collocation methods have proven to be an efficient discretization scheme for many aerodynamic (see e.g. [5-9]) and fluid mechanic (e.g. [10-13]) problems. The higher-order accuracy and resolution shown by these methods allows one to obtain engineering-accuracy solution on coarse meshes, or alternatively, to obtain solutions with very small error. There exist, however, drawbacks to spectral techniques which prevent their

widespread usage. One drawback to these techniques has been the requirement that a complicated physical domain must map onto a simple computational domain for discretization. This mapping must be smooth if the high-order accuracy and exponential convergence rates associated with spectral methods are to be preserved [6]. Additionally, even smooth stretching transformations can decrease the accuracy of a spectral method, if the stretching is severe [9]. Such stretchings would be required to resolve the thin viscous region in an external aerodynamic problem, or the widely disparate scales which occur in chemically-reacting flows. Furthermore, problems with discontinuities in boundary conditions, very high-gradient regions or shocks cause oscillations in the spectral solution. The above situations are more the rule than the exception in hypersonic flows.

These restrictions are overcome in the present method by splitting the domain into regions, each of which preserve the advantages of spectral collocation, and allow the ratio of the mesh spacings between regions to be several orders of magnitude higher than allowable in a single domain [14]. Adjoining regions are interfaced by enforcing a global flux balance which preserves high-order continuity of the solution. This interface technique maintains spectral accuracy, even when mappings and/or domain sizes are radically different across the interface, provided that the discretization in each individual subdomain adequately resolves the solution there.

Spectral flux balance interface technique. A simple one-dimensional, two-region example will serve to illustrate the present method for interfacing two collocation-discretized regions. Given the second order, potentially nonlinear boundary-value problem:

$$\begin{aligned} &[F(U)]_x - \nu U_{xx} = S(U), && x \in [-1, 1], \\ &U(-1) = a, && U(1) = b, \end{aligned} \tag{1}$$

We wish to place an interface at the point $x = m$, and have independent collocation discretization in the regions $x^{(1)} \in [-1, m]$ and $x^{(2)} \in [m, 1]$. Even though the point $x = m$ is an interior point to the problem domain, simply applying a collocation statement there, utilizing a combination of the discretizations on either side, will not work; the resulting algebraic system is singular. This is because the spectral second-derivative operator has two zero eigenvalues; thus the patching together of two spectrally-discretized domains yields potentially four zero eigenvalues in the overall algebraic system. Two of these eigenvalues are accounted

for by imposition of boundary conditions, and one by continuity of the solution at the interface leaving one zero eigenvalue in the system. To alleviate this difficulty, a global statement of flux balance is used. Rewriting (1) as:

$$[G(U)]_x = S(U) \tag{2}$$

where the flux is

$$G(U) = F(U) - \nu U_x, \tag{3}$$

then integrating (2) from -1 to 1 results in

$$G(U)\big|_{x=1} - G(U)\big|_{x=-1} + [G]\big|_{x=m} = \int_{-1}^{1} S(U)dx. \tag{4}$$

If the jump in flux at the interface, [G], is zero, then (4) may be written:

$$G(U)\big|_{x=-1} + \int_{-1}^{m} S(U)\, dx = G(U)\big|_{x=1} - \int_{m}^{1} (U)\, dx. \tag{5}$$

The statement of global flux balance across the two regions, along with the assumption that the solution is continuous, provides the condition necessary to close the equation set which results from spectral discretization of (1) in two regions. Note that the left side of (5) involves the discretization in the region $x^{(1)} \in [-1, m]$ while the right side involves the region $x^{(2)} \in [m, 1]$. Since spectral collocation discretization strongly couples all points in their respective regions, (5) couples all points in both discretizations.

Note also that no statement is made concerning whether or not (1) is advection- or diffusion-dominated. Equation (1) is considered a scalar equation here, although the above is extendable to a system.

3. Numerical Model of Nonequilibrium Shock Flow. The above technique will model the chemical kinetics and flow kinematics of a nonionized air mixture (02, N2, NO, O, and N) passing through a fully resolved shock wave, thus alleviating the need for artificial viscosity. The governing equations are the quasi-one dimensional Navier-Stokes equations [15], and species conservation equations [16]. The quasi one-dimensional form is used to provide an artifice for controlling the shock location in the physical space for this otherwise indeterminate problem.

The conservation equations can be written as:

$$\frac{\partial U}{\partial t} + \frac{\partial F}{\partial x} = \frac{\partial V}{\partial x} + W \qquad (6)$$

where the dependent variables are denoted by U, the convective flux by F, the dissipative flux by V, and the production rate by W. The equations are nondimensionalized by dividing the state and transport parameters by their dimensional free-stream values. Each of the quantities U, F, V, and W, have 8 components. These expressions are given explicitly in Appendix A.

The viscosity of each of the individual species is calculated from a curve fit relation [17]. Similarly, curve fits are used to obtain specific heats internal energies, and enthalpies [18,19]. The thermal conductivity of each specie is calculated from the Euken semi-empirical formula using the specie's viscosity and specific heat. Appropriate mixture rules are next used to obtain the transport properties of the mixture [20]. Experimental values of bulk viscosities, as obtained from acoustical interferometry and related experiments, are taken from Truesdell [21].

In the present work, the diffusion model is limited to binary diffusion with the binary diffusion coefficients specified by the Lewis number. The value of the Lewis number used is 1.4.

The temperature range under study will not exceed 8000 Kelvin, for conditions at an altitude of approximately 190,000 feet. Therefore, ionization reactions, which occur at roughly 9000 Kelvin, are not included. The chemical reactions utilized for the nonionized air mixture are impact dissociation and exchange reactions. The seventeen reactions included in the present study can be found in ref. 16, which also lists ionization reactions. The constants needed to evaluate reaction rates are given in ref. [16].

Initial conditions are obtained from a spectral multi-domain code for solution of the Navier-Stokes equations with equilibrium chemistry, written for the above problem. These governing equations may be found in ref 15. Transport properties are obtained in the manner previously discussed. The routines of ref. 18 generalized for air are used to obtain equilibrium concentrations.

Compressible multi-domain algorithm. The multi-domain discretization involves three independent subdomains, with the shock located in the center subdomain. Shock jump conditions are obtained by an iterative procedure to solve the Rankine-Hugoniot relations for real air.

A direct inversion of the coupled system is utilized to obtain a fully implicit method. The conserved variables are written in delta form, and a pseudo time iteration using backwards Euler is utilized to obtain the steady state solution as follows. Time-local linearization of equation (6) leads to the implicit form of the equation over the time step Δt:

$$\left\{I + \Delta t\left[\frac{\partial}{\partial x}\left(A + \frac{\partial B}{\partial x}\right) - \frac{\partial^2}{\partial x^2} B - S\right]\right\}\Delta U = \Delta t\left[W + \frac{\partial}{\partial x}(-F + V)\right] \tag{7}$$

where I is the unit matrix, and A, B, and S are Jacobian matrices: $A = \partial(F-V)/\partial U$, $B = \partial(F-V)/\partial U_x$, and $S = \partial W/\partial U$. These Jacobians are obtained analytically and are evaluated at the previous time step. Because of the large rank and ill-condition of the Jacobian matrix, iterative improvement of the Gaussian elimination solution was found to be required. Nonetheless the scheme required less than one second per time step on the Cray-2 at NASA Ames for typical discretizations used in this study.

Method verification. Validity of the multi-domain Navier-Stokes algorithm is demonstrated by comparison with experiment. A low-density wind tunnel study of shock-wave structure and relaxation phenomena in gases was conducted by Sherman [22]. The experiment measured shock wave profiles recorded in terms of the variation in the equilibrium temperature of a small diameter wire oriented parallel to the plane of the shock, as the wire is moved through the shock zone. Free stream Mach number is 1.98. For this test case, a Navier-Stokes spectral multi-domain calculation is performed for a perfect gas with temperature-dependent properties and a nonzero bulk viscosity corresponding to air [21]. A comparison with experimental temperatures normalized by the free stream temperature versus normalized distance is given in figure 1. The experimental data points are represented by the open symbols. The numerical results fall within a symbol width of the data. The multi-domain technique utilized three domains. The center domain, located between $x = -.15$, and $x = 0.3$, contains 21 points; the outer domains contain 11 points each. The computational domain spans -1 to 1. The unit Reynolds number of the flow is 80. A calculation for a unit Reynolds number of 1000 is given in figure 2, showing the ability of the method to accurately resolve strong gradients without numerical oscillations. The plot is of Mach number versus normalized distance. Three domains are again used; the center domain contains 17 points and the outer domains contain 11 points each with the interfaces located at -.15 and -.1.

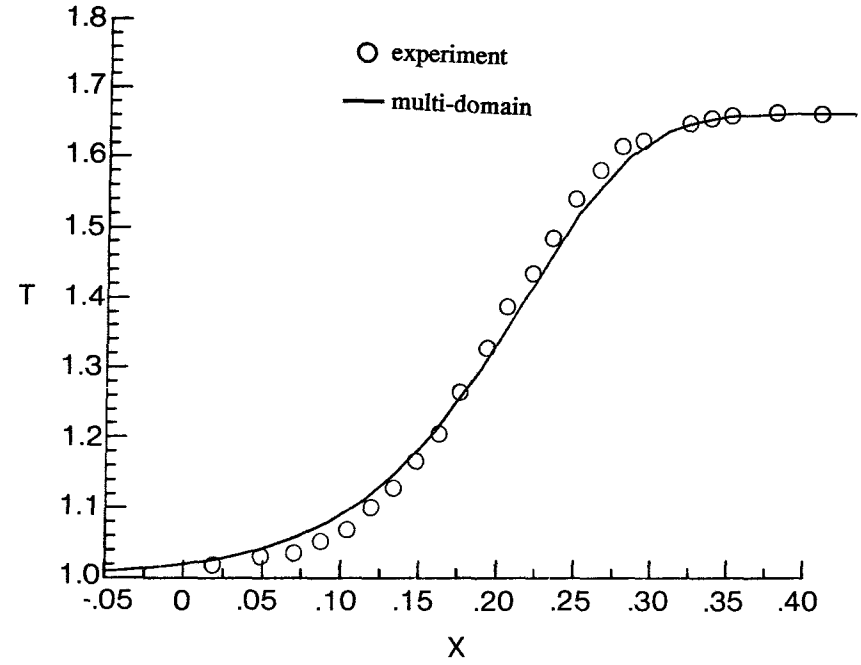

Figure 1. Comparison of multi-domain Navier-Stokes calculation with experimentally obtained temperatures; $M_\infty = 1.98$, Re = 80. Discretization 11/21/11, interfaces at -.15 and .3.

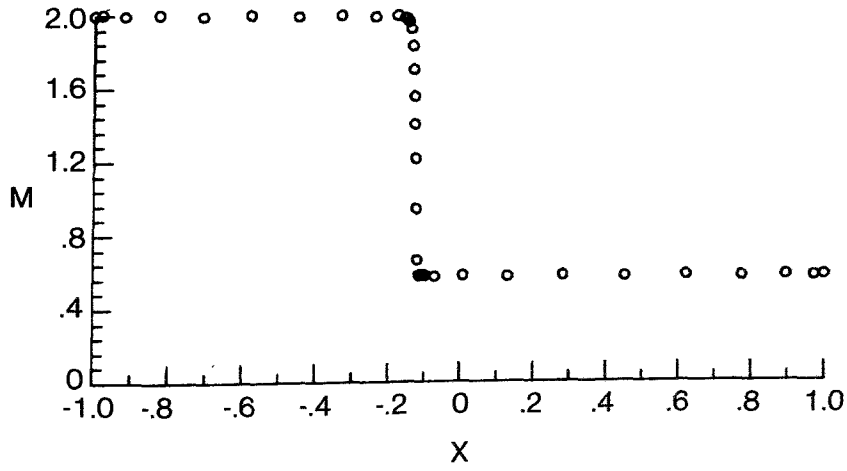

Figure 2. - Computed solution for Re = 1000; discretization 11/17/11, interface at -.15 and -.1.

Results. The method is used to calculate the chemical kinetics initiated as air passes through a hypersonic shock wave. The case to be discussed for nonequilibrium flow is $M_\infty = 11.0$, $T_\infty = 350K$, and $\rho_\infty = 6 \times 10^{-8} g/cm^3$. These conditions invoke primarily O_2 dissociations with N_2 dissociations just beginning. Temperatures are not yet high enough for ionization to occur, so electronic energy modes remain unexcited.

Typical discretizations used in this study were 15, 27 and 33 points in the upstream, middle and downstream domains, respectively. The backward-Euler implicit time-stepping algorithm typically required less than 2000 iterations to converge from an equilibrium starting solution, with at least an eight order of magnitude reduction in maximum residual.

A study of the effect of artificial visosity on the flow physics was carried out by adding the equivalent of second-order artificial viscosity to the momentum, energy, and species' concentration equations. The amount of artifical viscosity introduced was such that the shock was spread out to a thickness about three orders of magnitude wider than the fully-resolved no artificial viscosity solution. This width was chosen to represent the grid spacing of a typical shock-capturing computation on a full-scale configuration. Figures 3a and 3b show the Mach number and temperature profiles for the resolved-shock and smeared-shock cases respectively; note that the entire physical domain is shown in Fig. 3b, whereas only the near-shock region on a greatly expanded scale is plotted in Fig. 3a. For the resolved-shock case, endpoints are at -1 and 200, and interface points are at -.3 and .1. The interface locations for the smeared shock case are at 65 and 100, with endpoints at 0 and 270. The most important feature to note in comparing these profiles is the 20% reduction in the temperature overshoot as a result of the artificial viscosity. In a calcuation with ionization, such a reduction could prevent its onset; or similarly, a calculation with combustion chemistry may not reach threshold temperatures necessary for ignition due to this artificial damping. In addition, the high temperature zone following the passage of air through the shock persists for roughly two orders of magnitude downstream further than the resolved shock case. Computationally, this effect of artificial viscosity could cause a chemical reaction to produce more of a given species than what occurs in the true physics.

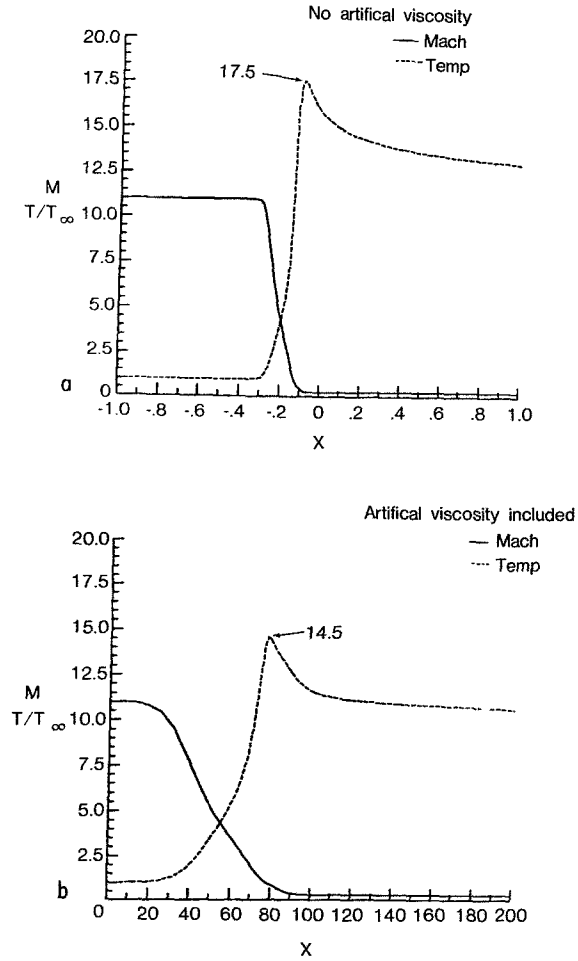

Figure 3. - Comparison of temperature and Mach number profiles for calculations; (a) without artificial viscosity, and (b) with artificial viscosity.

For the Mach 11 case considered here, although the path along which the chemistry relaxes is significantly altered in the near-shock region, the chemical end states from the computations with and without artificial viscosity are within 3-4% of each other. This can be seen in Figs. 4a,b which show the profiles for [N] and [NO] in the relaxation zone. This is not to say, however, that this situation will always occur especially for higher Mach numbers where electronic excitation (ionization) occurs. The reduction in the temperature overshoot could result in a large enough change in the relaxation path that the end state could be affected significantly.

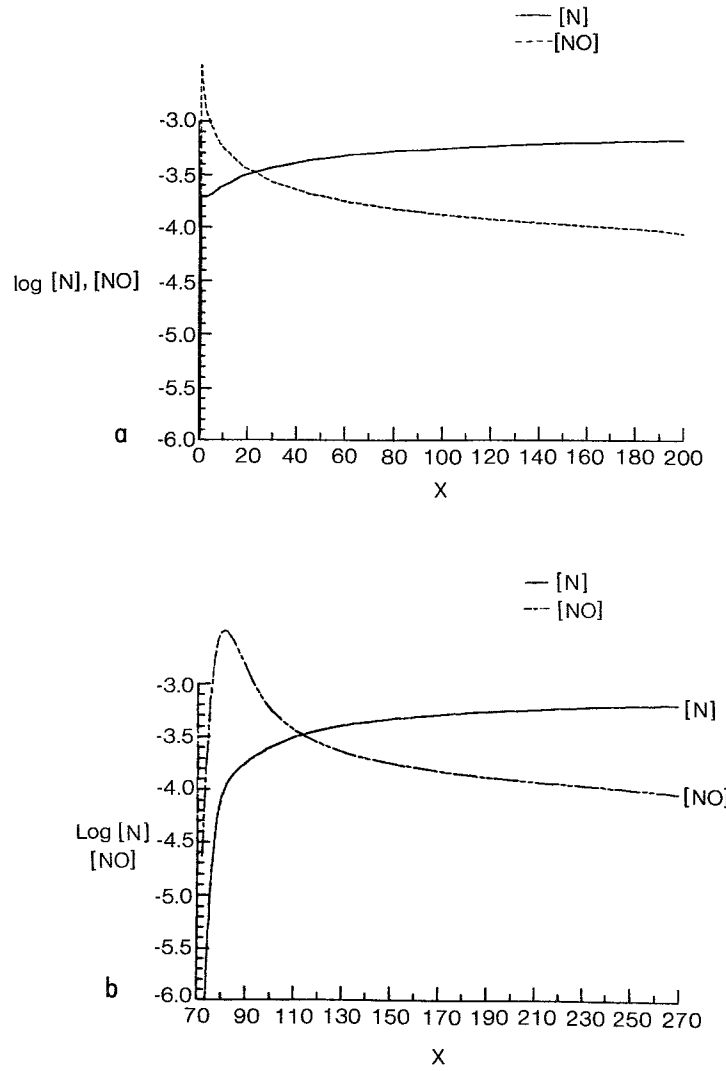

Figure 4. - Comparison of relaxation pathway for [N] and [NO] from calculations; (a) without artificial viscosity, and (b) with artificial viscosity.

4. Stability of Compressible Flows. The second focus is a careful study of the stability of high-speed boundary layers and free-shear flows. A newly developed spectral stability code (staggered pressure mesh) is presented for analysis of compressible viscous flow stability. An order of magnitude less number of points is needed for equivalent accuracy of growth rates compared to those calculated by a finite-difference formulation. Supersonic disturbances which are found to have highly irregular structures have been resolved by a spectral

multi-domain discretization, which requires a factor of three fewer points than the single domain spectral stability code.

At the present time, there is no prospect of a unified theory of transition even in low speed flows (where some of the underlying mechanisms are relatively well-known), let alone in hypersonic flows. As a short-term goal, it is imperative then to obtain linear stability results. The implicit assumption is that supersonic/hypersonic transition has its origin in linear instability and is not overly sensitive to details of the disturbance environment (not that Morkovin's bypasses are inapplicable to the hypersonic regime). Clearly, as Mack [23] points out, there is a need to develop efficient, accurate and robust linear stability codes for use in a large number of design calculations.

This is the motivation behind the present work which treats the linear compressible stability equations by a spectral collocation method. Results are presented to substantiate these claims. Furthermore, the multi-domain version of this method presented here deals economically with complex flows which can include such features as multiple interior shear layers. This section first validates the method for the case of boundary layers and free shear layers, then goes on to present some new results in the case of free mixing layers.

Formulation of compressible stability equations. The basic equations governing the flow of a viscous compressible fluid are the Navier-Stokes equations. For this stability study, the equations in Appendix A, modified for a perfect gas, describes the system.

In this study all velocities are scaled by U_e, the x component of velocity at the edge of the boundary layer, and all lengths are scaled by δ^*, the displacement thickness of the velocity profile in the x-direction. The Reynolds number and Mach number are given by

$$Re = \frac{U_e \delta^*}{\nu_e} \tag{8}$$

$$M = \frac{U_e}{\sqrt{\gamma}\, Re\, T_e} \tag{9}$$

where ν_e and T_e are the kinematic viscosity and mean temperature in the freestream, and gamma is the ratio of specific heats. The results in the present paper consider σ = Prandtl number = .72 and $\bar{\mu}^*$ is evaluated by Sutherland's law.

If we assume that the base flow is a locally parallel boundary layer then

$$u(x,y,z,t) = U_o(y) + \hat{u}(y)e^{i(\alpha x+\beta z-\omega t)} \quad (10)$$

$$v(x,y,z,t) = \hat{v}(y)\, e^{i(\alpha x+\beta z-\omega t)} \quad (11)$$

$$w(x,y,z,t) = W_o(y) + \hat{w}(y)e^{i(\alpha x+\beta z-\omega t)} \quad (12)$$

$$p(x,y,z,t) = \hat{p}(y)\, e^{i(\alpha x+\beta z-\omega t)} \quad (13)$$

$$\tau(x,y,z,t) = T_o(y) + \hat{\tau}(y)e^{i(\alpha x+\beta z-\omega t)} \quad (14)$$

where U_o, W_o, and T_o represent the steady unperturbed boundary layer (mean flow), and quantities with tildas denote complex disturbance amplitudes. $V_o(y)$ is assumed zero since the flow is parallel, and $P_o(y)$ is zero since pressure is assumed constant across the boundary layer. α and β are x and z disturbance wave numbers, respectively, and ω is the complex frequency. Equations (10)-(14) are substituted into he nondimensional Navier-Stokes equations, the mean flow terms subtracted out, and the terms which are quadratic in the disturbance neglected. The resulting system is the linearized compressible Navier-Stokes equations for the disturbance quantities as given in Appendix B.

Solution technique. The equations in Appendix B constitute an eigenvalue problem for the complex frequency ω, once the disturbance wavenumbers α and β are specified. Discretization of these equations in the y-direction forms a generalized matrix eigenvalue problem, suitable for computer solution. Equations (B1)-(B7) are essentially an eighth order system; thus the eight boundary conditions (eq. (B7)) are sufficient for solution, and no boundary condition is applied to the disturbance pressure. Whatever discretization scheme is used must respect this arrangement if an accurate solution is to be expected.

The discretization scheme used here is a spectral collocation technique, using Chebyshev polynomials as basis functions. The nodes of the variables $\hat{v}$, $q^+ = \alpha\hat{u} + \beta\hat{w}$, $q^- = \alpha\hat{w} - \beta\hat{u}$, and $\hat{\tau}$ are located at the Gauss-Lobatto points (the extrema of the last retained Chebyshev polynomial [24]); the energy and momentum equations are collocated at these points. Thus discrete boundary conditions may be imposed for these variables at both end points of the domain. The pressure nodes are located at the Gauss points (the zeroes of the first neglected polynomial) of a Chebyshev series one order less than that used for the other variables; the continuity equation is collocated at these points. Since no Gauss points fall on the boundary, we are free of any

requirement of providing an artificial numerical boundary condition for pressure, and we have the proper balance of number of equations and unknowns.

The farfield boundary of the discretized domain is placed at a finite distance, typically 20-100 δ^* from the wall or shear-layer centerline. Extensive sensitivity studies were performed to determine the effect of this finite domain truncation.

Stretching is employed in the discretization to improve resolution near the wall/centerline. In the case of the boundary layer, either of two stretching forms are used:

$$y_p = y_{max}(C_2 - 1)^{C_1} y_c/(C_2 - y_c^2)^{C_1} \tag{15}$$

or

$$y_p = y_{max}\, C_3 y_c/(1 + C_3 - y_c) \tag{16}$$

where y_p is the coordinate in the physical space $[0,y_{max}]$, y_c is the computational coordinate ε $[0,1]$, and C_1, C_2, and C_3 are adjustable constants. In this work, C_1 is either 4 or 6, and C_2 ranged from 1.2 to 2.0; C_3 is used between .01 and .03. For the shear layer, equation (15) is used as the stretching, yielding a physical space of $[-y_{max}, y_{max}]$ from $y_c \varepsilon$ $[-1,1]$.

Using standard spectral collocation discretization formulas [24], matrix differentiation operators are formed for both the Gauss-Lobatto ($\hat{v}$, q+, q-, $\hat{\tau}$) and the Gauss ($\hat{p}$) grids, incorporating the selected stretching function. Mean flow quantities from the spectral boundary layer code of [25] are spectrally interpolated onto the new mesh, and derivatives of these quantities obtained using the differentiation operators. The generalized matrix eigenvalue problem which results from this discretization is of the form:

$$A_{GL}L_{GL}^2\vec{\phi} + B_{GL}L_{GL}(\vec{\phi} + I_G^{GL}P) + C_{GL}(\vec{\phi} + I_G^{GL}P) = \omega[D_{GL}L_{GL}(\vec{\phi} + I_G^{GL}P) + E_{GL}(\vec{\phi} + I_G^{GL}P)] \tag{17}$$

for the momentum and energy equations, and

$$B_G L_G \, I_{GL}^{G} \vec{\phi} + C_G \left(I_{GL}^{G} \vec{\phi} + P \right) = \omega E_G \left(I_G^{GL} \vec{\phi} + P \right) \qquad (18)$$

for the continuity equation, where A, B, C, D, and E are matrix coefficients derived from equations (B1)-(B5), L denotes a spectral differentiation operator, the unknown vector $\phi = (\hat{v}, q^+, q^-, \hat{\tau})^T$, and the vector P contains the disturbance pressure $\hat{p}$. Subscripts GL and G denote location at or operation on Gauss-Lobatto and Gauss point grids, respectively; I_G^{GL} and I_{GL}^{G} are spectral interpolation matrices from Gauss to Gauss-Lobatto points and vice-versa.

The unknown vectors $\vec{\phi}$ and P are collected into a single vector, and the matrix equations (17) and (18) are assembled into a large generalized matrix eigenvalue problem for input into a standard library routine for solution. A complex modified QZ algorithm [26] is used to obtain the eigenvalues of the system directly; this is referred to as a global search. The most unstable eigenvalue is then selected, and used as an input to an inverse Rayleigh method to purify the eigenvalue of the effects of round-off error and to obtain the solution eigenvectors. In all cases, the global and local (Rayleigh-iterated) eigenvalues agreed to better than eight decimal places.

Verification.

Boundary layer. For verification, calculations are performed for the stability analysis of compressible two-dimensional similarity boundary layer profiles. A spectral mean flow code modified for compressible flow is used for this purpose [25].

A Mach number boundary layer profile perturbed by a three dimensional disturbance at $M_\infty = 4.5$, $T_e = 520°R$, $Re = 10{,}000$, $\alpha = .6$, $\beta = 1.0392$ is first analyzed. A resolution study for the eigenvalue computations are given in Tables I and II for the single domain spectral code and COSAL (a finite-difference compressible stability code, [27]), respectively. Roughly 3 significant digits for values of growth rate are obtained with the spectral code using 81 points; in Table II COSAL is seen to require approximately 800 points for equivalent accuracy. Eigenfunctions for $\hat{u}$ are shown in Fig. 5a,b from each code. A multi-domain spectral discretization (MDSPD) with two domains obtains equivalent accuracy with the single domain spectral stability code with 1/3 the number of points, as illustrated in Table III. The savings is significant considering that the number of operations in the spectral stability code goes as the cube of the number of points.

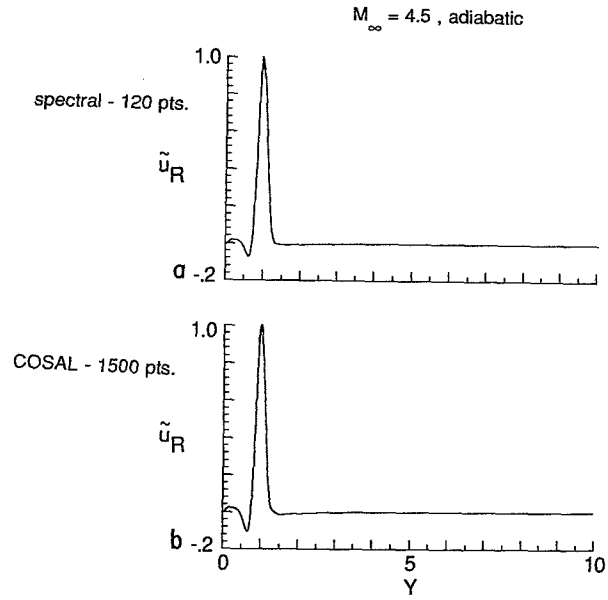

Figure 5. - $\hat{u}$-velocity fluctuation amplitude function for $\alpha = .6$, $\beta = 1.0392$, $M_\infty = 4.5$, $Re = 10{,}000$, $T_e = 520°R$. Calculation by:
a. Spectral stability code
b. COSAL

The reason for the increased efficiency with the MDSPD is that in addition to the significant structure at the wall (Fig. 5), the farfield boundary must be far enough out so that the exponential rate of decay associated with these disturbances is accurately captured. For this case, the outer extent is 30 displacement thickness units (y coordinate) from the wall at y = 0 to capture this exponential decay, otherwise the accuracy of the growth rate is effected. These issue put a severe demand on the stretching required for resolution with a single-domain discretization. The multi-domain utilized two domains with interface at 2. The inner domain has 25 points and is unstretched; the outer domain has 17 points and a tanh stretching.

Stability of a Viscous, Compressible Shear Layer. The spectral stability code is used to analize the stability of a viscous, compressible shear flow obtained from a spectral similarity solution obtained by modifying the boundary-layer code of ref. 25. The shear flow consists of two parallel gases: an injected stream into a quiescent gas. Issues of relevance in this study is understanding the impact of transition on fuel/air mixing efficiency in scramjet combustors. It has been observed

experimentally that the mixing efficiency is decreased fourfold in the range of Mach 1 to 4. The cause of this trend is unkown. However, it is well known that turbulent mixing is many orders of magnitude faster than laminar. Ideally one would like to be able to manipulate the downstream evolution of shear layers to enhance mixing -- perhaps linear stability theory holds a clue. The initial stages of shear flow instabilities are driven by linear mechanisms which persist for a considerable distance downstream. Understanding the growth and propagation of the disturbance in these early stages will allow not only a better understanding of the onset of transition, but will allow initiation of the transition process in a numerical model so that the physics might be systematically studied. This study investigates a range of Mach numbers, gas temperatures and disturbance wave numbers. The mean flow in all cases involves a jet being injected into a quiescent gas.

It is observed that the disturbance eigenfunctions significantly tighten in structure as α increases which puts a greater demand on the resolution required for a single domain spectral discretization (SDSPD). A progression of eigenfunction plots for increasing α (phase angle $\theta = 60°$) is given in Figs. 6 and 7 illustrating this observation.

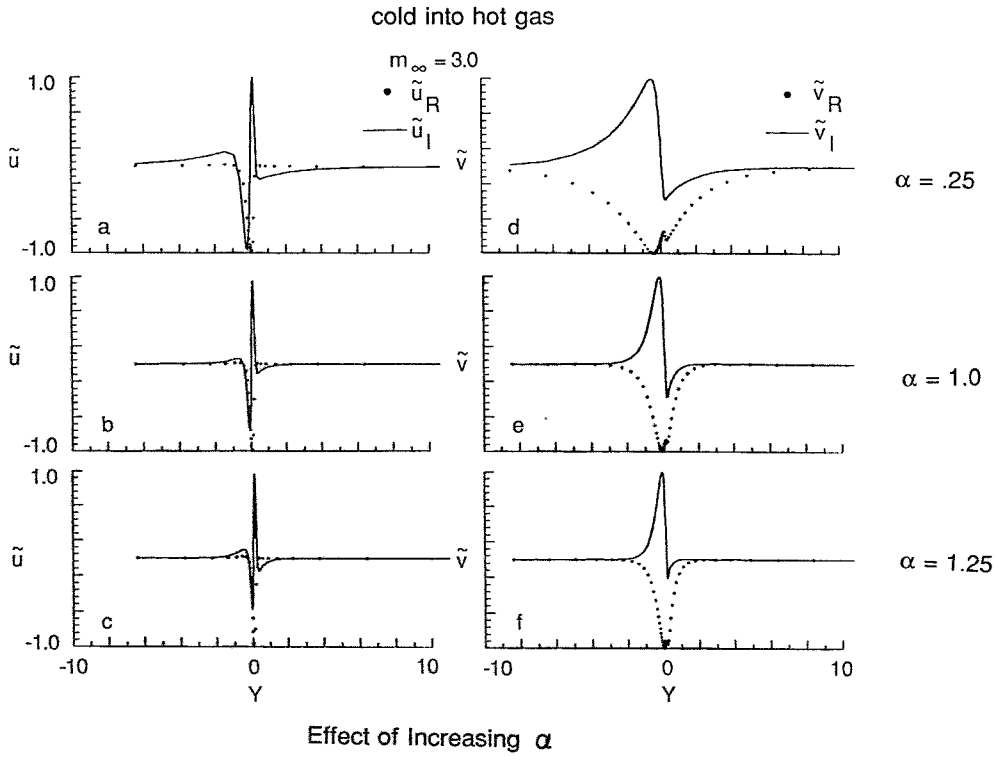

Figure 6. - Effect of increasing α on $\hat{u}$ and $\hat{v}$ eigenfunctions; $\theta = 60°$, $M_\infty = 3$.

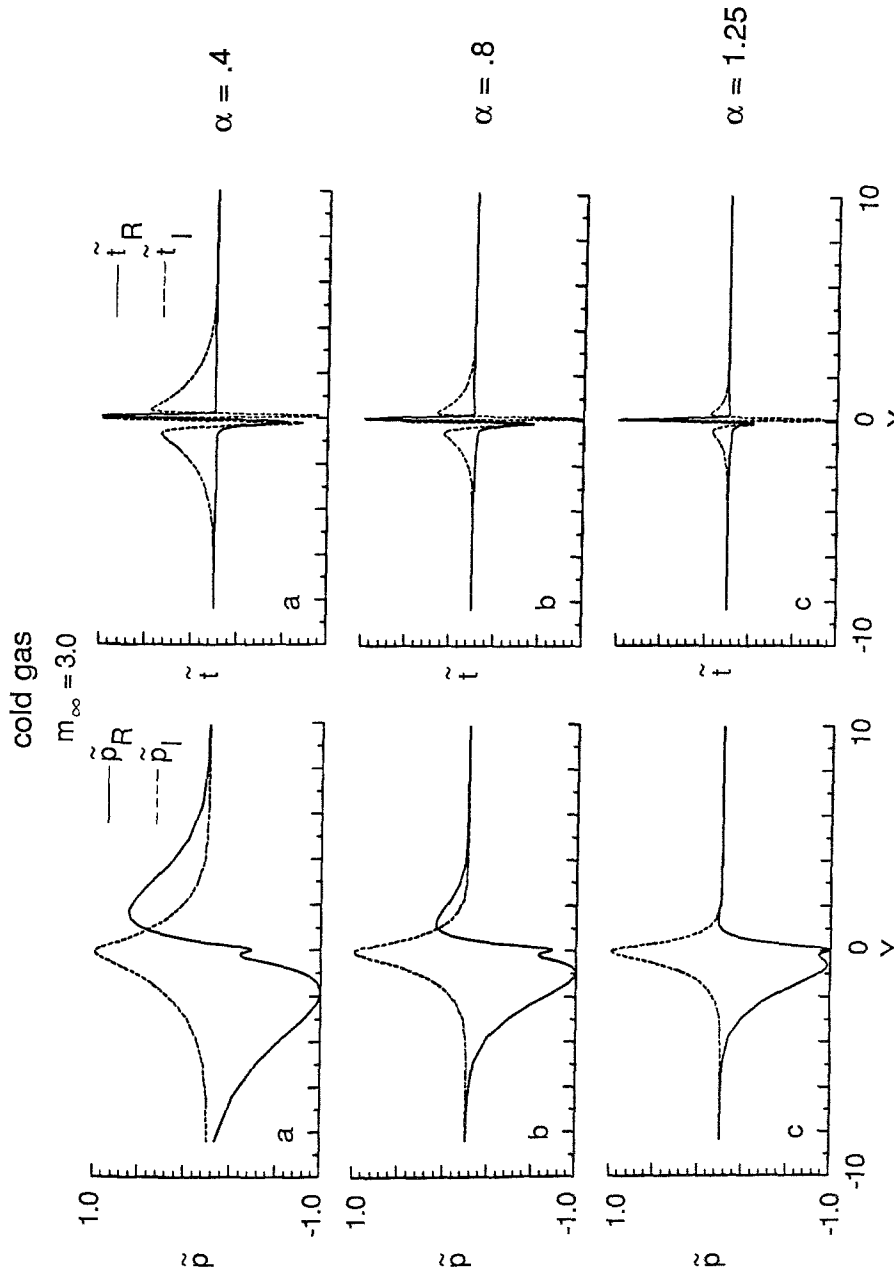

Figure 7. - Effect of increasing α on $\tilde{p}$ and $\tilde{t}$ eigenfunctions; $\theta = 60°$, $M_\infty = 3$.

Difficulties in resolution similarly occur for higher Mach number disturbances. The spectral stability code had difficulty resolving eigenfunctions beyond 3.75 for the cold injection cases and as early as Mach 3 for the hot injection case for disturbance wave angles of 60°. Restrictions on the allowable stretching for single domain spectral methods contributes to this difficulty. Examples of the MDSPD for cases requiring a very severe stretching will be given later.

The above studies involve three dimensional disturbances with a wave propagation angle of 60°. Preliminary

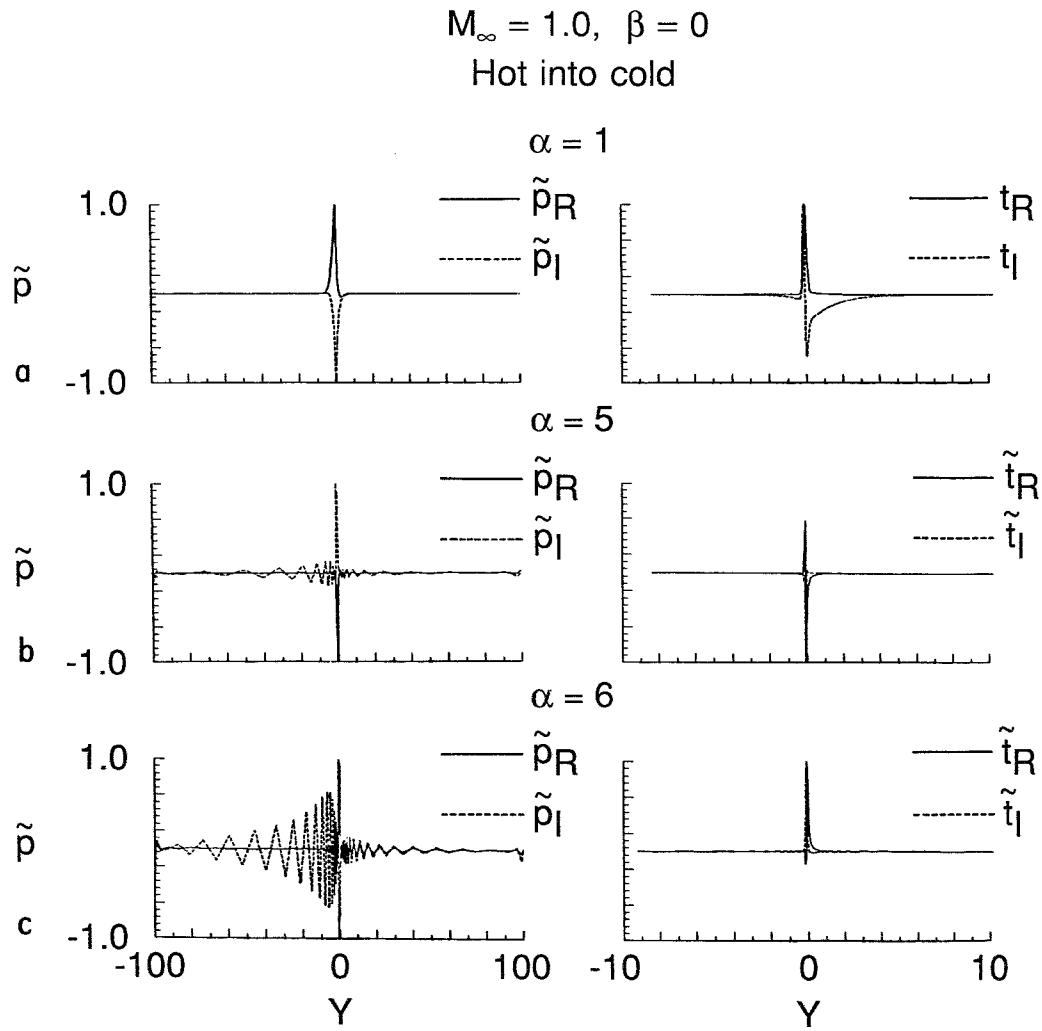

Figure 8. - Effect of increasing α on $\hat{p}$ and $\hat{t}$ disturbance eigenfunctions; $M_\infty = 1$, $\beta = 0$, Re = 10,000.
a. $\alpha = 1$.
b. $\alpha = 5$.
c. $\alpha = 6$.

results indicate that two dimensional disturbances ($\beta = 0$) exhibit similar trends; however, difficulties in resolving eigenfunctions with a SDSPD occur at lower Mach numbers. Again at higher α disturbance eigenfunctions tighten radically beyond the limit at which a single domain spectral method can resolve; the hardest temperature case to resolve is hot injection into a colder gas. This observation is demonstrated in Fig. 8 which plots a sequence of $\hat{p}$ and $\hat{t}$ eigenfunction for increasing α, $\beta = 0$. The mean flow corresponds to $M_\infty = 1$, $Re = 10{,}000$ with $\beta_T = .2$ ($\beta_T = T_{quiescent}/T_{injected}$). Note the extremely tight structures in $\hat{p}$ and $\hat{t}$ as α increases. Note that $\hat{t}$ is plotted on the interval [-10,10], the actual spatial extent is [-100,100]. Oscillations in $\hat{p}$ for $\alpha = 5$ and 6 are quite pronounced.

The MDSPD resolves these cases with relative ease. To illustrate this point, $\hat{p}$ and $\hat{v}$ eigenfunctions obtained from the MDSPD are displayed in Fig. 9 for the

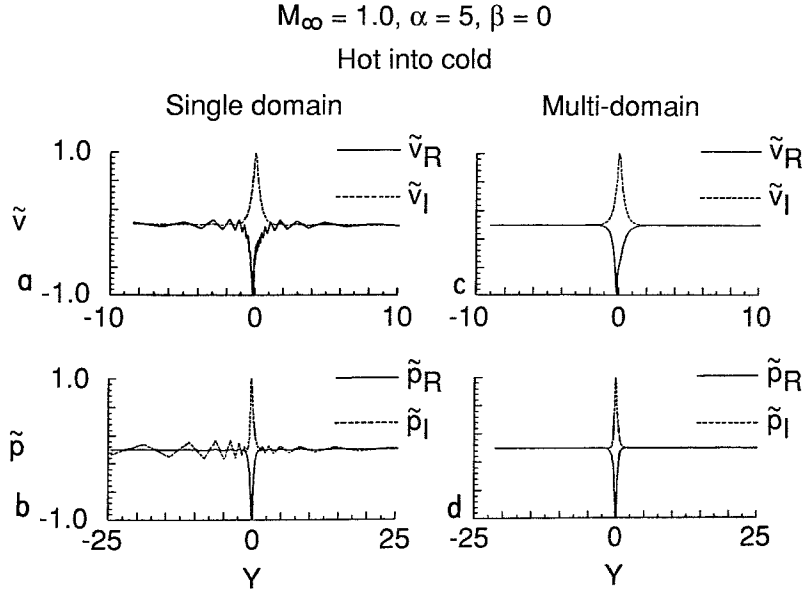

Figure 9. - $\hat{v}$ and $\hat{p}$ eigenfunctions obtained with spectral multi-domain discretization as opposed to single domain spectral discretization for case described in Fig. 8, $\alpha = 5$.

single domain:	multi-domain:
a. $\hat{v}$	c. $\hat{v}$
b. $\hat{p}$	d. $\hat{p}$

Re = 10,000, α = 5 case discussed previously. Adjacent to the multi-domain results are the single domain solution for $\hat{p}$ and $\hat{v}$. The multi-domain solution remains oscillation free. The number of points in each discretization is roughly 100, however, the multi-domain utilizes three domains, with 41 points in the center domain between -.5 and .5, 25 points in the left domain between -100. and -.5, and 37 points in the right domain between .5 and 100. The plot of the pressure disturbance for the entire spatial extent obtained from the multi-domain solution is given in Fig. 10, to illustrate the fineness of the structure which is resolved.

The preceding case (α = 5) is found to be resolvable by a SDSPD but only after quite a bit of trial and error stretching of the mesh for a variety of resolutions. The important point is that the MDSPD is quite robust and gives accurate eigenvalues over a wide range of stretching parameters. This observation is illustrated in Table IV which lists a range of stretching parameters and corresponding phase speeds and growth rates for the preceding case. Both the SDSPD and MDSPD for this illustration utilized 99 points with the same outer extent. Note that for the SPSPD cases changing the

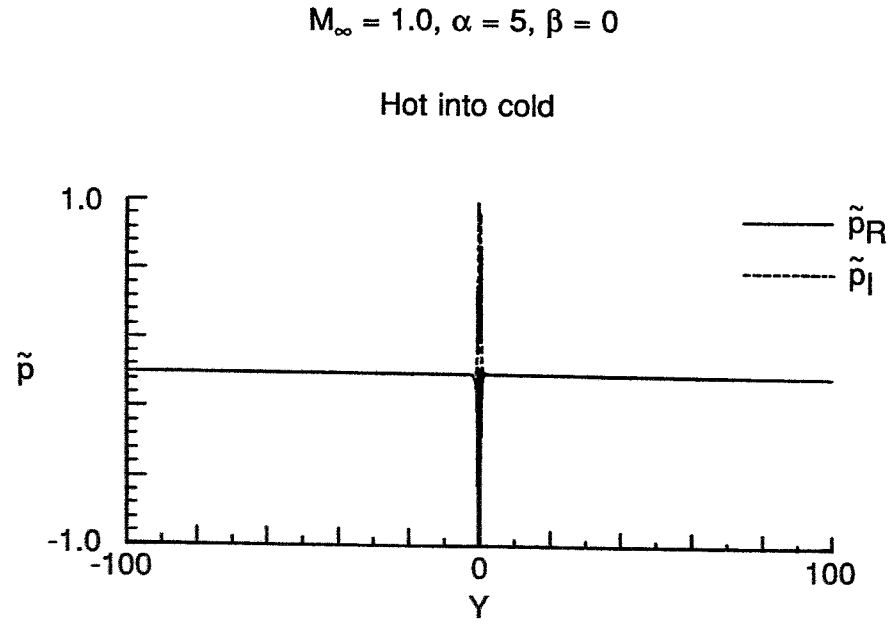

Figure 10. $\hat{p}$ disturbance eigenfunctions obtained by multi-domain stability code displayed on entire computational domain for case of Fig. 9. Discretization: center domain on [-.5,5], 41 pts.; left domain on [-100,-.5], 21 pts.; right domain on [.5,100], 35 pts.

stretching parameter by approximately 25% causes about a 10% change in phase speed and over a 50% change of value in growth rate. Contrast this sensitivity with the MDSPD cases. The stretching parameter is allowed to vary 100% in the center domain (three domains are utilized with interfaces at ±1). The phase speed has changed by less than 1% and the growth rate by only 6%. This robustness is extremely important since one usually has no idea of the value of the phase speed or growth rate. In addition, one needs to determine whether the disturbance mode is spurious--which is measured by its persistance over a wide range of resolutions.

As mentioned earlier, the disturbance eigenfunctions become increasingly complex as Mach number is increased. These higher Mach number cases are unresolvable by a SDSPD. To illustrate, a series of $\hat{p}$ and $\hat{v}$ eigenfunctions calculated by the SDSPD stability code are displayed in Fig. 11 and 12, respectively, for a disturbance wave angle of 60°. Note that at $M_\infty = 3.5$ the injected gas side of the disturbance begins to take on an oscillatory nature; at $M_\infty = 3.75$ these oscillations are more pronounced. It is well known that for supersonic disturbances the eigenfunction structure will be oscillatory [29]. (A supersonic disturbance occurs when the wave velocity of the disturbance relative to the local flow, in the direction of wave propagation, has a magnitude greater than the speed of sound.) The MDSPD is able to capture the structure of these supersonic modes with relative ease. Fig. 13 displays two unstable

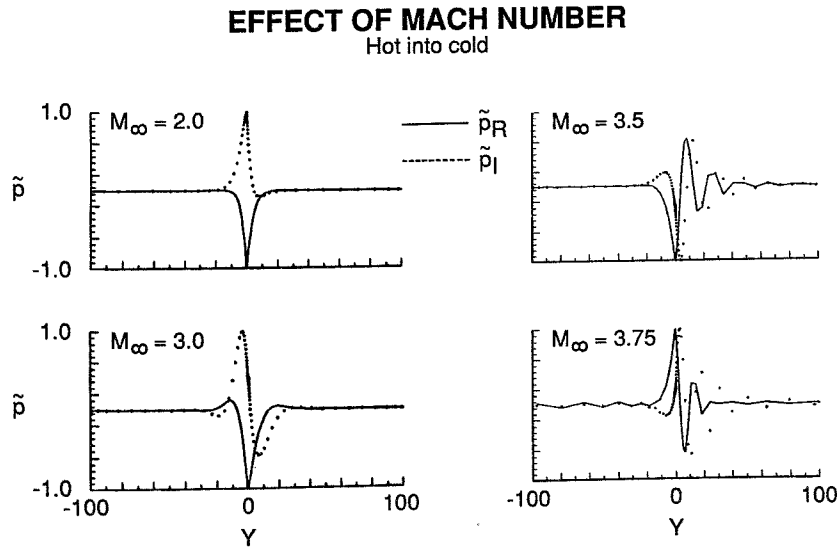

Figure 11.- $\hat{p}$ disturbance eigenfunctions for increasing Mach number and a SDSPD ($\theta = 60°$).

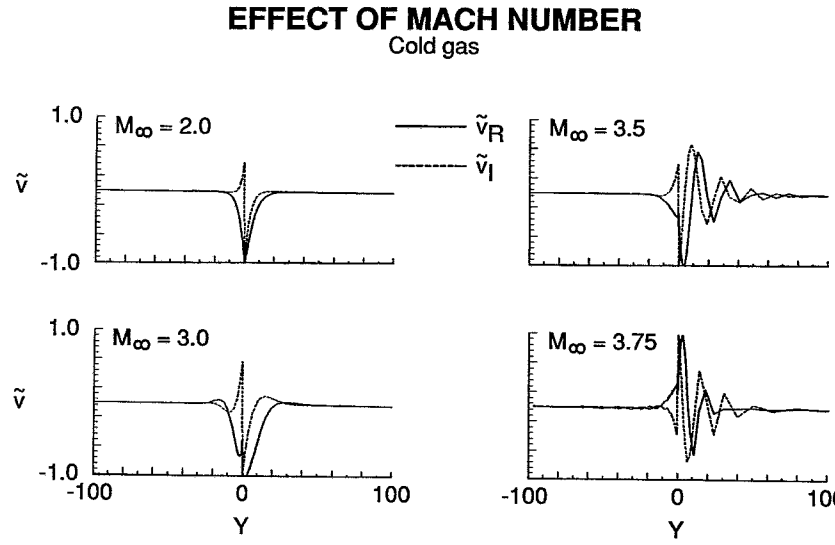

Figure 12.- $\hat{v}$ disturbance eigenfunctions for increasing Mach number and a SDSPD (θ = 60°).

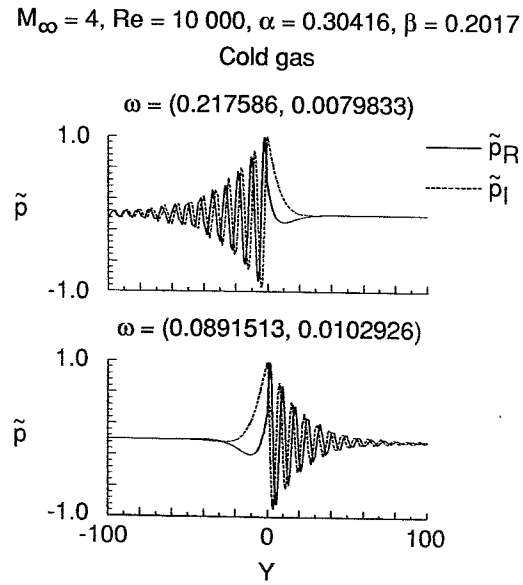

Figure 13.- $\hat{p}$ disturbance eigenfunctions for two unstable supersonic modes corresponding to a M_∞ = 4; ;Re = 10,000; θ = 60°. MDSPD with three domains: 41/105/41, interface at ±1.

supersonic modes which are associated with the instability of a Mach 4, $\beta_T = 1$, free shear flow. The disturbance wave numbers are $\alpha = .30416$, and $\beta_T = .2017$. The MDSPD involves three domains: 105 points on the oscillatory side, 41 points in the inner domain, and 41 points in the outer domain where the profile is smooth. Interface locations are located at ±1. Note further the level of complexity of the $\hat{t}$ eigenfunctions of this case. Fig. 14 is a plot of $\hat{t}$ for both modes on a full scale ±100 and greatly expanded scale ±1. The center structure is an added complexity to the structure which also requires adequate resolution, and further illustrated the necessity of a flexible discretization scheme like a MDSPD.

Conclusions. The present global flux balance spectral multi-domain method has demonstrated maintenance of exponential-order accuracy on a variety of advection- and diffusion-dominated test problems [14]. Extremely large differences in discretization across an interface through domain size, number of points and stretchings, have been shown to not disrupt this property of the present method. Additionally, this technique can be used to isolate certain types of coefficient, mapping, or boundary condition discontinuities.

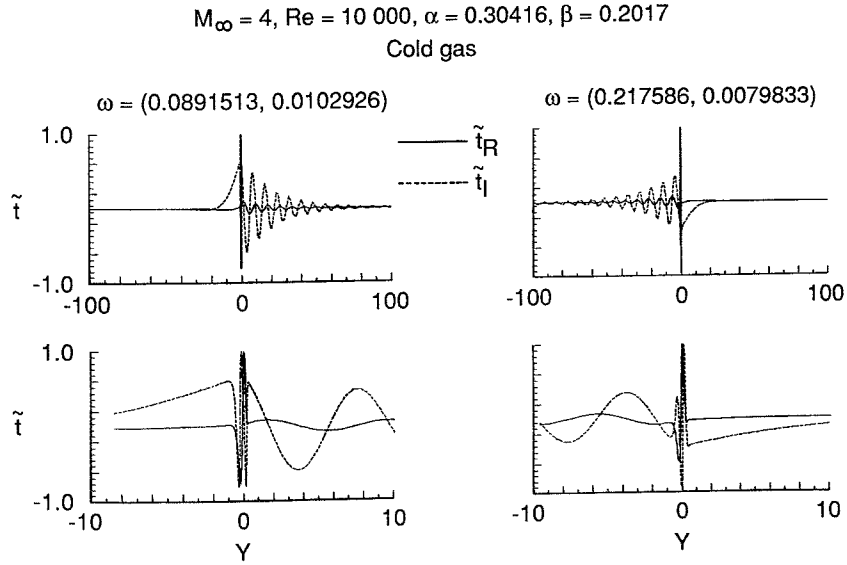

Figure 14.- $\hat{t}$ disturbance eigenfunctions for two unstable supersonic modes corresponding to a $M_\infty = 4$; Re = 10,000; $\theta = 60^0$, on a full scale (±100) and greatly expanded scale (±1). MDSPD: 41/105/41, interface at ±1.

These advantages have made possible the first compressible Navier-Stokes calculation by a spectral multi-domain technique. In addition, a Mach 11 shock calculation with nonequilibrium chemistry was performed to study the chemical kinetics initiated as air passes through a fully-resolved shock wave.

In addition, the first spectral collocation linear stability code for compressible flow is presented. The accurate discretization (staggered pressure grid) may be carried over to nonlinear simulations. Verification cases for high-speed boundary layers indicate an order of magnitude reduction in the number of points required for a single domain spectral discretization (SDSPD) to obtain equivalent accuracy in growth rates with a finite-difference formulation. In addition, a multi-domain spectral discretization (MDSPD) is found to require a factor of three less points man the (SDSPD), which is significant since the operation count of the spectral formulation goes as the cube of the number of points.

The first viscous stability analysis of a compressible shear flow is presented. The study indicates that for subsonic disturbances stability ofmixing layers is enhanced by viscosity, increasing Mach number and higher temperatures of the injected gas. Disturbances become supersonic at lower Mach numbers for 2-D disturbances ($M < 2$). 3-D disturbances become supersonic in the Mach number range of 3.5 to 4. The exact value of this Mach number depends upon the value of β_T the lower the value of β_T (cooling) the lower the Mach number at which the disturbance eigenfunctions become supersonic. The highly irregular structure of the supersonic modes are easily resolved by MDSPD stability code which is shown to be highly robust over a wide range of stretching parameters and resolutions.

Appendix A. Non-equilibrium one-dimensional Navier-Stokes equations

$$\frac{\partial U}{\partial \tau} + \frac{\partial F}{\partial x} = \frac{\partial V}{\partial x} + W \tag{A1}$$

Conservation variables

$$U_i = \rho\gamma_i, \quad 1 < i < NS, \text{ number of species} \tag{A2}$$

$$U_{NS+1} = \rho \tag{A3}$$

$$U_{NS+2} = \rho u \tag{A4}$$

$$U_{NS+3} = \rho E \tag{A5}$$

Convective fluxes

$$F_i = uU_i, \quad 1 \leq i \leq NS \tag{A6}$$

$$F_{NS+1} = \rho u \tag{A7}$$

$$F_{NS+2} = \rho u^2 + P \tag{A8}$$

$$F_{NS+3} = (E + P)u \tag{A9}$$

Viscous fluxes

$$V_i = \frac{Le}{Pr\ Re}\ \mu\ \frac{\partial \gamma_i}{\partial x}, \quad 1 \leq i \leq NS \tag{A10}$$

$$V_{NS+1} = 0 \tag{A11}$$

$$V_{NS+2} = \frac{(\lambda + 2\mu)}{Re}\ \frac{\partial \rho u}{\partial x} \tag{A12}$$

$$V_{NS+3}$$

$$= \frac{(\lambda + 2\mu)}{Re}\ u\ \frac{\partial \rho u}{\partial x} + \frac{\beta\ k}{(\beta - 1)\ Pr\ Re}\ \frac{\partial}{\partial x}\left[(\beta - 1)\left\{E - \frac{u^2}{2}\right\}\right]/z$$

$$+ \left[\frac{1 - \beta}{z}\right]\frac{Le\ m_\infty}{Pr\ Re}\left[E - \frac{\rho u^2}{2}\right]\ \sum_{i=1}^{NS} h_i\ \frac{\partial}{\partial x}\gamma_i \tag{A13}$$

where

m_∞ = freestream molecular weight

Le = Lewis number
z = compressibility: $P = z\ \rho\ T$

h_i = enthalpy of species "i"

$\beta = h/e$

Source production terms

$$W_i = \sum_{r=1}^{NR} (\beta_{i,r} - \alpha_{i,r})\left[R_r^f - R_r^b\right] \tag{A14}$$

$$R_r^f = k_r^f \prod_{J=1}^{NS} (\rho\gamma_j)^{\alpha_{j,r}} \qquad R_r^b = k_r^b \prod_{j=1}^{NS} (\rho\gamma_j)^{\beta_{j,r}} \tag{A15}$$

$$k_r^f = A_1\ T^{A_2} \exp(-A_3/T) \qquad k_r^b = B_1\ T^{\beta_2} \exp(-B_3/T) \tag{A16}$$

NR = number of reactions

$\alpha_{i,r}$, $\beta_{i,r}$ = stoichiometric coef. for forward and backward reactions, resp.

$W_{NS+1} = W_{NS+2} = W_{NS+3} = 0$

Appendix B. Linearized compressible Navier-Stokes stability equations.

$$D^2(\alpha\hat{u} + \beta\hat{w}) + \frac{1}{\mu_o}\frac{d\mu_o}{dT_o}T_o'D(\alpha\hat{u} + \beta\hat{w}) + i(\lambda - 1)(\alpha^2 + \beta^2)(\alpha\hat{u} + \beta\hat{w}) - \left[\frac{Re}{\mu_o T_o}(\alpha U_o' + \beta W_o') - \frac{i}{\mu_o}\frac{d\mu_o}{dT_o}T_o'(\alpha^2 + \beta^2)\right]\hat{v} - \frac{iRe}{\mu_o}(\alpha^2 + \beta^2)\hat{p} = 0 \quad (B1)$$

$$D^2\hat{v} + \frac{i(\lambda-1)}{\lambda}D(\alpha\hat{u} + \beta\hat{w}) - \left[\frac{iRe}{\mu_o T_o \lambda}(\alpha U_o + \beta W_o - \omega) + \frac{\alpha^2 + \beta^2}{\lambda}\hat{v} + \frac{i}{\lambda\mu_o}\frac{d\mu_o}{dT_o}(\alpha U_o' + \beta W_o')(\alpha\hat{w} - \beta\hat{u}) = 0 \quad (B2)$$

$$D\hat{v} + i(\alpha\hat{u} + \beta\hat{w}) - \frac{T_o'}{T_o}\hat{v} + i\gamma M^2(\alpha U_o + \beta W_o - \omega)\hat{p} - \frac{i}{T_o}(\alpha U_o + \beta W_o - \omega)\hat{\tau} = 0 \quad (B3)$$

$$D^2\hat{\tau} + 2(\gamma - 1)M^2\sigma\frac{(\alpha V_o' + \beta W_o')}{\alpha^2 + \beta^2}D(\alpha\hat{u} + \beta\hat{w}) + \frac{2i}{\mu_o T_o'}\frac{d\mu_o}{dT_o}D\hat{\tau} + 2(\gamma-1)M^2\sigma\frac{(\alpha W_o' - \beta U_o')}{(\alpha^2+\beta^2)}D(\alpha\hat{w} - \beta\hat{u}) - \left[\frac{Re}{\mu_o T_o}T_o' - 2i(\gamma-1)M^2\sigma(\alpha U_o' + \beta W_o')\right]\hat{v} + \frac{iRe\sigma}{\mu_o}(\sigma-1)M^2(\alpha U_o + \beta W_o - \omega)\hat{p} - \left[\frac{iRe\sigma}{\mu_o T_o}(\alpha U_o + \beta W_o - \omega) + (\alpha^2+\beta^2) - (\gamma-1)\frac{\sigma M^2}{\mu_o}\frac{d\mu_o}{dT_o}(U_o'^2 + W_o'^2) - \frac{1}{\mu_o}\frac{d^2\mu_o}{dT_o^2}(T_o')^2 - \frac{1}{\mu_o}T_o''\frac{d\mu_o}{dT_o}\right]\hat{\tau} = 0 \quad (B4)$$

$$D^2(\alpha\hat{w} - \beta\hat{u}) + \frac{1}{\mu_o}\frac{d\mu_o}{dT_o}(\alpha W_o' - \beta U_o')D\tau' + \frac{1}{\mu_o}\frac{d\mu_o}{dT_o}T_o'D(\alpha\hat{w} - \beta\hat{u}) - \frac{Re}{\mu_o T_o}(\alpha W_o' - \beta U_o')\hat{v} + \left[\frac{T_o'}{\mu_o}\frac{d^2\mu_o}{dT_o^2}(\alpha W_o' - \beta U_o') + \frac{1}{\mu_o}\frac{d\mu_o}{dT_o}(\alpha W_o'' - \beta U_o'')\right]\hat{\tau}$$

$$-\left[\frac{iRe}{\mu_o T_o}(\alpha U_o + \beta W_o - \omega) + (\alpha^2 + \beta^2)\right](\alpha\hat{w} - \beta\hat{u}) = 0 \qquad \text{(B5)}$$

Where primed quantities indicate differentiation with respect to y. The equation of state is where ϕ_o is the mean flow density and $\hat{\phi}$ the complex density disturbance. The boundary conditions are

$$(\hat{v},\ \alpha\hat{u} + \beta\hat{w},\ \alpha\hat{w} - \beta\hat{u},\ \hat{\tau}) = 0 \quad @ \quad y = 0$$

$$(\hat{v},\ \alpha\hat{u} + \beta\hat{w},\ \alpha\hat{w} - \beta\hat{u},\ \hat{\tau}) \to 0 \quad \text{as } y \to \infty \qquad \text{(B7)}$$

Table I. Calculation of temporal eigenvalues for different grids using spectral stability code.

($M_\infty = 4.5$, $T_e = 520°R$, Re = 10,000, $\alpha = .6$, $\beta = 1.0392$)

# pts	ω
45	(.531703936, $1.835681668 \times 10^{-2}$)
51	(.495671735, $3.892834157 \times 10^{-3}$)
63	(.495719127, $3.903565212 \times 10^{-3}$)
65	(.495936719, $3.890656057 \times 10^{-3}$)
73	(.495844598, $3.977529728 \times 10^{-3}$)
81	(.495811969, $3.933484970 \times 10^{-3}$)
95	(.495825367, $3.933674615 \times 10^{-3}$)
120	(.495824177, $3.935165423 \times 10^{-3}$)
151	(.495824195, $3.935192776 \times 10^{-3}$)
200	(.495824195, $3.935192907 \times 10^{-3}$)

Table II. Calculation of temporal eigenvalues for different grids using COSAL

($M_\infty = 4.5$, $T_e = 520°R$, $R_e = 10,000$, $\alpha = .6$, $\beta = 1.0392$)

# pts	ω
211	(.485935455, $3.720663427 \times 10^{-3}$)
513	(.495990048, $3.688194736 \times 10^{-3}$)
1025	(.495983122, $3.683247436 \times 10^{-3}$)
1500	(.495981891, $3.682367822 \times 10^{-3}$)
1500 (with Richardson extrapolation)	(.495980770, $3.681512173 \times 10^{-3}$)

Table III. Calculation of temporal eigenvalues for different grids using multi-domain spectral stability code.

(M_∞ = 4.5, T_e = 520^{0}R, Re = 10,000, α = .6, β = 1.0392)

2 Domains (total # of points)	ω	
25/17 (42)	.495824525	3.935144920 x 10^{-3}
31/21 (52)	.495824188	3.935209430 x 10^{-3}
37/21 (58)	.495824191	3.935210299 x 10^{-3}

Table IV. Effect of stretching parameter: single vs. multi-domain spectral discretization

(M_∞ = 1.0, Re = 10,000, β_T = .2, α = 5, β = 0)

Single-domain, 99 pts. on [-100, 100]

Stretching Parameter	ω	
1.1	1.47179	.272236
1.2	1.49883	.159461
1.3	1.49806	.158226
1.4	1.57814	.266635

Multi-Domain, 17/65/17 (99 pts) on [-100/-1/1/100]

Stretching Parameter	ω	
1.6	1.497268	.167511
2.0	1.496913	.159498
2.2	1.497146	.158781
4.0	1.496359	.156986

References

[1] A.T. Patera, A spectral element method for fluid dynamics: laminar flow in a channel expansion. J. Comput. Physics 54 (1984).

[2] N. Ghaddar, A.T. Patera and B. Mikic, Heat transfer enhancement in oscillatory flow in a grooved channel, AIAA Paper 84-0495.

[3] B. Metivet and Y. Morchoisne, Multi-domain spectral techniques for viscous flow calculations, in: Proceedings of the 4th Conference on Numerical Methods in Fluid Dynamics, Oct. 1981.

[4] H.H. Migliore and E.G. McReynolds, Multi-element collocation solution for convective dominated transport, C. Taylor, J. Johnson, and W. Smith, Eds., Numerical Methods in Laminar and Turbulent Flow, 1983.

[5] D.L. Gottlieb, L. Lustman and C.L. Streett, Sectral methods for two-dimensional shocks, ICASE Report No. 82-83, Nov. 1982.

[6] C.L. Streett, A spectral method for the solution of transonic potential flow about an arbitrary two-dimensional airfoil, AIAA Paper No. 83-1949-CP, Paper presented at the AIAA 16th Computational Fluid Dynamics Conference, Danvers, MA, July 13-15, 1983.

[7] M.Y. Hussaini, C.L. Streett and T. Zang, Spectral methods for partial differential equations, NASA CR-172248, Aug. 1983.

[8] C.L. Streett, T.A. Zang and M. Hussaini, Spectral multigrid methods with applications to transonic potential flow, Comput. Physics 56 (1984).

[9] C.L. Streett, T.A. Zang, and M.Y. Hussaini, Spectral methods for solution of the boundary-layer equation, AIAA Paper 84-0170, Paper presented at the AIAA 22nd Aerospace Sciences Meeting, Reno, NV, Jan. 9-12, 1984.

[10] M.G. Macaraeg, Numerical model of the axisymmetric flow in a heated, rotating spherical shell, PhD Dissertation, University of Tennessee Space Institute, TX 1-541-627, June 1984.

[11] M.G. Macaraeg, The effect of power law body forces on a thermally-driven fluid between concentric rotating spheres, J. Atmospheric Sci. 62 (2) (1986).

[12] M.G. Macaraeg, A mixed pseudospectral/finite difference method for the axisymmetric flow in a heated, rotating spherical shell, J. Comput. Physics 43 (3) (1986).

[13] M.G. Macaraeg, A mixed pseudospectral/finite difference method for a thermally-driven fluid in a nonuniform gravitational field, AIAA Paper 85-1662, Present at the AIAA 18th Fluid Dynamics and Plasmadynamics and Laser Conference, Cincinnati, OH, July 15-18, 1985.

[14] M.G. Macaraeg, and C.L. Streett, Improvements in Spectral Collocation Discretization Through a Multiple Domain Technique, Applied Numerical Mathematics, vol. 2, no. 2, 1986.

[15] W.C. Davy, C.K. Lombard, and M.J. Green, Forebody and Base Real-Gas Flow in Severe Planetary Entry by a Factored Implicit Numerical Method, AIAA Paper 81-0282.

[16] C. Park, On Convergence of Computation of Chemically Reacting Flows, AIAA Paper 85-0247.

[17] F.G. Blottner, Nonequilibrium Laminar Boundary Layer Flow of Ionized Air, General Electric Report R645D56, 1964.

[18] W.D. Erickson, and R.K. Prabhu, Rapid Combustion of Chemical Equilibrium Composition: An Application to Hydrocarbon Combustion, AIChE Journal, vol. 32, 1986.

[19] Janaf Tables, Thermochemical Data - Dow Chemical Co., 1977.

[20] R.B. Bird, W.E. Stewart, and E.N. Lightfoot, Transport Phenomena, 1966.

[21] C. Truesdell, Precise Theory of the Absorption and Dispersion of Forces Plan Infinitesimal Waves According to the Navier-Stokes Equations, J. of Rational Mechanics and Analysis, vol. 2, no. 4, 1953.

[22] F.S. Sherman, A Low Density Wind-Tunnel Study of Shock Wave Structure and Relaxation Phenomena in Gases, NACA TN-3298, 1955.

[23] Mack, L. M., "Boundary Layer Stability Theory," NASA CR-131591 (Jet Propulsion Lab.), November 1969.

[24] Streett, C. L., "Spectral Methods and their Implementation to Solution of Aerodynamic and Fluid Mechanic Problems," presented at the Sixth International Symposium on Finite Element in Flow Problems, Antibes, France, June 1986.

[25] Streett, C. L., T. A. Zang, and M. Y. Hussaini, "Spectral Methods for Solution of the Boundary-Layers Equations," AIAA paper no. 84-0170, presented at the 22nd AIAA Aerospace Sciences Meeting, Reno, Nevada, January 1983.

[26] Wilkinson, J. H.: The Algebraic Eigenvalue Problem. Oxford, 1965.

[27] Malik, M. R., "COSAL - A Black-Box Compressible Stability Code for Transition Prediction in Three-Dimensional Boundary Layers," NASA CR-165925, May 1982.

[28] Drummond, J. P., "Numerical Simulation of a Supersonic, Chemically Reacting Mixing Layer," PhD dissertation, George Washington University, May 1987.

[29] Gropengiesser, H.: Study of the Stability of Boundary Layers and Compressible Fluids. NASA TT F-12,786, 1969.